Available online at www.sciencedirect.com
SCIENCE DIRECT®
Journal of Power Sources 132 (2004) 315–320
JOURNAL OF POWER SOURCES
www.elsevier.com/locate/jpowsour

Synthesis and electrochemical characterization of amorphous MnO_2 electrochemical capacitor electrode material

Ravinder N. Reddy, Ramana G. Reddy*

Department of Metallurgical and Materials Engineering, The University of Alabama, P.O. Box 870202, Tuscaloosa, AL 35487 0202, USA

Received 4 December 2003; received in revised form 20 December 2003; accepted 20 December 2003

Abstract

Amorphous MnO_2 was synthesized using the sol–gel method by reduction of $NaMnO_4$ with solid fumaric acid. The synthesized product was characterized using X-ray diffraction, scanning electron microscopy, thermogravimetric analysis, BET and chemical analysis. Electrochemical characterization was performed using cyclic voltammetry by a three electrode method, and aqueous NaCl, KCl, and Na_2SO_4 solutions were used as electrolytes. Prepared material remained amorphous until 400 °C and transformed to crystalline Mn_2O_3 at 500 °C. The composition of prepared material was determined to be $Na_{0.25}MnO_2{\cdot}0.5H_2O$. A maximum capacitance of 110 F/g was obtained at a scan rate of 5 mV/s in 2 M NaCl solution. MnO_2 yielded almost the same capacitance in 2 M and 1 M NaCl electrolytes. The specific capacitance of MnO_2 remained constant up to 800 cycles in 1 M NaCl electrolyte at 5 mV/s scan rate.

Keywords: Amorphous MnO_2; Sol–gel; Electrochemical capacitors

1. Introduction

Electrochemical capacitors (ECs) are gaining momentum as energy storage devices due to their higher power density and longer cycle life compared to batteries and higher energy density than conventional dielectric capacitors [1–5]. They have useful applications as back up and pulse power sources for many electronic devices. Recently, they have become of interest in hybrid electric vehicles as an auxiliary power source in combination with a fuel cell or battery. The role of the EC in hybrid electric vehicles is load leveling, start-up and acceleration. Depending on the charge storage mechanism, ECs are categorized as electrochemical double layer capacitors (EDLC) and pseudocapacitors. The origin of capacitance in the EDLC is charge separation at the electrode–electrolyte interface, whereas pseudocapacitance arises from fast, reversible faradiac redox reactions taking place on or near the surface of the electrode. The capacitance in an EDLC is of the order of tens and in psudocapacitor, it is the order of hundreds of μF per cm^2 of interfacial area [6].

MnO_2 appears to be a promising material due to its superior electrochemical performance, environmentally friendly nature and low cost. Various forms of MnO_2 have been extensively investigated for energy storage applications ranging from primary Zn/MnO_2 alkaline cells to lithium and lithium ion batteries [7]. Lately, much attention has been placed on MnO_2 as an electrode material for electrochemical capacitors [7–14]. In our previous study [2], we prepared MnO_2 as the electrode material. We prepared MnO_2 by reduction of sodium permanganate with disodium fumaric acid. In our studies we observed capacitance fading after 200 cycles. Capacitance fading was circumvented in our present study by preparing MnO_2 from different starting material. Yang et. al., [15] prepared MnO_2 by reduction of sodium permanganate with disodium fumaric acid and fumaric acid. In their studies, they monitored better surface properties for MnO_2 prepared from fumaric acid. The present authors have synthesized MnO_2 using the sol–gel method starting from sodium permanganate and fumaric acid and studied its electrochemical characteristics [16]. This papers deals with the details of the method of preparation of MnO_2 using the sol–gel method and examines its application as a potential electrode material for electrochemical capacitors.

2. Experimental

MnO_2 was synthesized by the sol–gel method as used by Franger et. al. [17]. The preparation involves reduction of sodium permanganate ($NaMnO_4$) with solid fumaric acid in

* Corresponding author. Tel.: +1-205-348-1740; fax: +1-205-348-2164.
E-mail address: rreddy@coe.eng.ua.edu (R.G. Reddy).

0378-7753/$ – see front matter © 2004 Elsevier B.V. All rights reserved.
doi:10.1016/j.jpowsour.2003.12.054

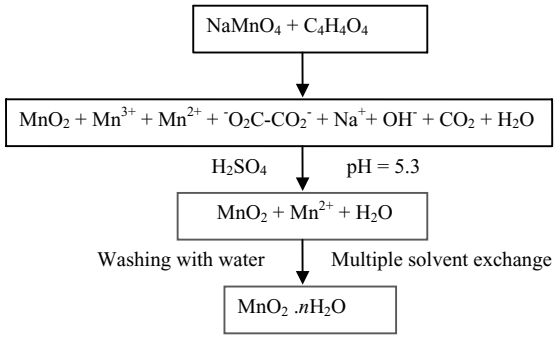

Fig. 1. Flow chart of preparation of ambigel form of MnO_2.

the mole ratio of 3:1. The reduction process illustrated as follows [17]:

$$3HOOCCH{=}CHCOOH + 10NaMnO_4 \rightarrow 10MnO_2 + 3Na_2C_2O_4 + 4NaOH + 4H_2O + 6CO_2 \uparrow$$

Mole ratio between sodium permanganate and fumaric acid is very critical to have effective oxidation state of the Mn in the final product to be around four. Solid fumaric acid was added in small amounts to the aqueous solution of $NaMnO_4$ while the solution was being stirred. Stirring was continued for one hour and the mixture was vacuum degassed later for 60 min to remove CO_2. The solution was stirred for 24 h and then H_2SO_4 was added slowly with stirring. The final pH of the solution was controlled to 5.3. The maintenance of pH around 5 is vital because the isoelectric point for MnO_2 is at pH 3 [18]. The solution was further stirred for 24 h and washed several times with distilled water to remove any soluble products. The final step was to remove water present along with the MnO_2. This step was achieved by exchanging the water with organic solvents. Details of this process were given in our previous paper [2]. Briefly, water present in the gel was stirred in acetone for 1 week. The acetone was replaced by cyclohexane and finally by hexane. The gel present in the hexane was dried under vacuum for 12 h at 60 °C. The dried product is called ambigel. Fig. 1 shows the preparation flow chart for the ambigel form of MnO_2.

3. Characterization

The products were characterized using various techniques such as X-ray diffractometry (XRD), scanning electron microscopy (SEM), Brunauer–Emmet–Teller (BET) method, inductively-coupled plasma emission spectrograph (ICP-ES) and thermogravimetric analysis (TGA/DTA). XRD was performed using the Philips PW3830 model. TGA was carried out using a Perkin-Elmer Pyris Diamond machine under ambient conditions with temperature increments of 10 °C/min. TGA data was used to find the amount of water present and also observe any structural transformations of MnO_2. The morphology of the synthesized powder was analyzed with Philips a XL30 scanning electron microscope. Surface area of the powder was determined by the BET method using Quanta Chrome, Chembet-3000 model. ICP-ES was used to determine the alkali ions present in the synthesized powder.

3.1. Electrode preparation and electrochemical characterization

The electrode material was prepared as in the similar way as described in our earlier paper [2] with 24 wt.% of carbon black and 9 wt.% PTFE binder. Sheets of approximate thickness of 125 μm were rolled. Approximately 10 mg of electrode material was utilized to conduct cyclic voltammetry using an EG&G potentiostat and galvanostat (273 A) employing the three electrode method. The procedure described in our earlier paper [2] was followed to carry out the CV experiments in NaCl, KCl, and Na_2SO_4 electrolytes with varying concentrations. A scan rate of 5 mV/s in the range of 0.0–1.0 V was applied in every measurement unless otherwise specified. All experiments were carried out at room temperature (25 °C). Specific capacitance (C) in F/g is calculated as anodic charge divided by voltage and normalized to one gram of active material.

$$C = \frac{1}{m\,\Delta V}\int_x^y i_a \mathrm{d}t \quad (1)$$

where i_a is the anodic current, t the time, x the time when $V = 0.0$ V, y the time when $V = 1.0$ V, ΔV the voltage range and m is the weight of the active material.

4. Results and discussion

Fig. 2a illustrates the XRD patterns of MnO_2 dried at different temperatures up to 400 °C. Lack of clear peaks and broadening of peaks indicate the amorphous nature. The amorphous nature was retained for the material dried at 400 °C. Fig. 2b shows the XRD patterns of MnO_2 dried at 500 and 650 °C. The patterns correspond to crystalline Mn_2O_3. Amorphous MnO_2 transformed to crystalline Mn_2O_3 at 500 °C and remained in the same phase until 650 °C. The surface area of as prepared material was found to be 83 m^2/g from BET analysis. Fig. 3a shows the TGA/DTA curves of the ambigel form of MnO_2. TGA depicted a total weight loss of 14% and a structural transformation. DTA displayed two exothermic peaks at 277 and 506 °C. The peak at 277 °C corresponds to the removal of chemically bound water and the peak at 506 °C corresponds to the transition of MnO_2 to Mn_2O_3 as determined by XRD. The composition of the prepared material from TGA/DTA and ICP analysis was determined to be $Na_{0.25}MnO_2{\cdot}0.5H_2O$. Fig. 3b indicates SEM image of MnO_2. Each particle consists of an agglomeration of small particles with an individual particle size of about 5 μm.

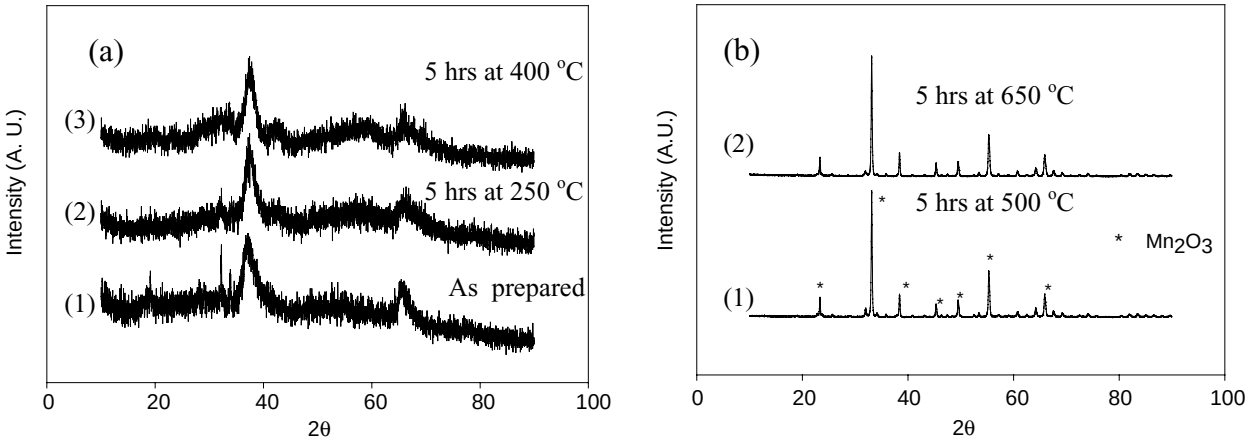

Fig. 2. XRD patterns of MnO_2 powder (a) (1) as prepared, (2) dried at 250 °C for 5 h, (3) dried at 400 °C for 5 h; (b) (1) dried at 500 °C for 5 h and (2) dried at 650 °C for 5 h.

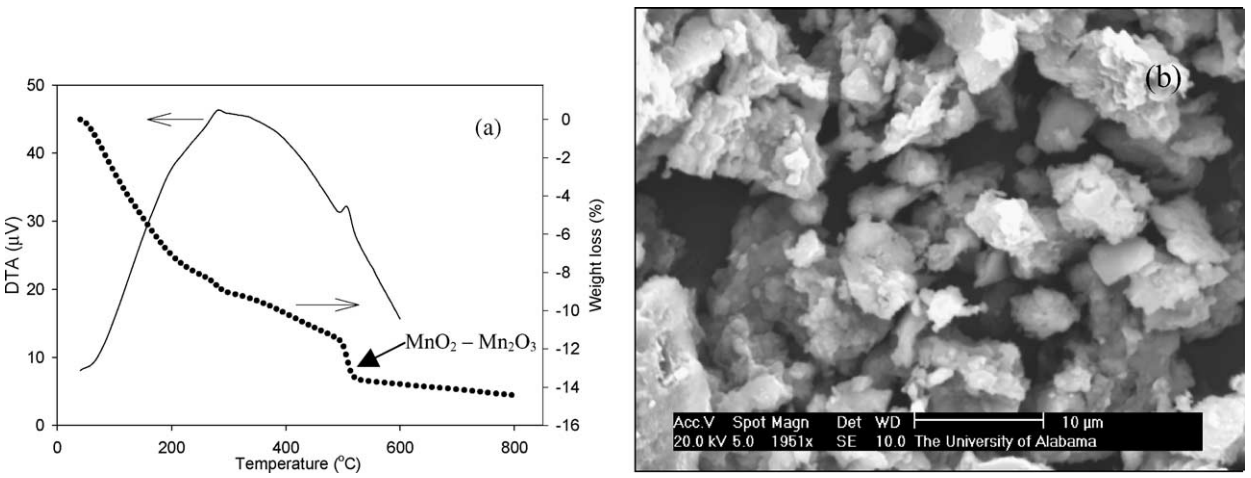

Fig. 3. (a) TGA (···) and DTA (—) curve of MnO_2. (b) SEM image of MnO_2.

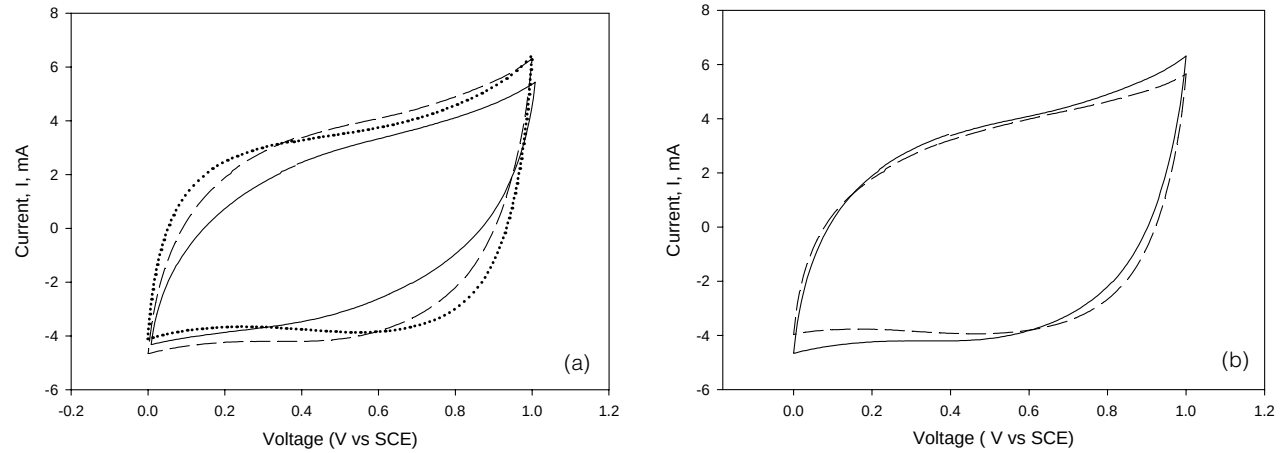

Fig. 4. CV curves of MnO_2 in (a) 2 M KCl (···), 2 M NaCl (- - -), 1 M Na_2SO_4 (—) electrolytes and (b) 2 M NaCl (—), 1 M NaCl (- - -) electrolytes.

Table 1
Specific capacitance of MnO_2 in different electrolytes with different concentrations

Electrolyte	Concentration (M)	Specific capacitance (F/g)
KCl	2	109
NaCl	2	110
NaCl	1	106
Na_2SO_4	1	93

4.1. Electrochemical characterization

4.1.1. Effect of electrolytes

Fig. 4a shows cyclic voltammetric (CV) curves of MnO_2 in 2 M KCl, 2 M NaCl and 1 M Na_2SO_4 electrolytes at 5 mV/s scan rate. Ideal capacitative behavior was observed in the cases of KCl and NaCl electrolytes. Despite the difference in the size of hydration sphere of sodium and potassium ions, MnO_2 yielded the same capacitance in 2 M KCl and NaCl electrolytes. In the case of Na_2SO_4, MnO_2 showed non capacitave behavior. When we compare the NaCl and Na_2SO_4 electrolyte, the only difference is the anion. Since the sulphate ion is bigger than the chloride ion, sodium ions might be hindered by bigger sulphate ions, which lead to non-capacitative behavior. The highest specific capacitance of 110 F/g was obtained in 2 M NaCl at 5 mV/s scan rate. Fig. 4b shows cyclic voltammetric curves of MnO_2 in 2 and 1 M NaCl at 5 mV/s scan rate. MnO_2 showed similar capacitance in both concentrations as evident from that figure. The specific capacitance of MnO_2 in different electrolytes is summarized in Table 1. Fig. 5 shows cyclic voltammetric curves of MnO_2 in 1 M NaCl electrolyte at different scan rates. At low scan rates (5 mV/s), the CV curve shows the near ideal rectangular shape. Non-capacitative nature was observed above 5 mV/s scan rate.

Fig. 6 shows the plot of voltammetric charges as a function of scan rate in 1 M NaCl electrolyte. The dependence of the voltammetric charge (q^*) of MnO_2 in 1 M NaCl solution on the scan rate can be understood by the slow diffusion of Na^+ ions into the pores of MnO_2 [14]. At high scan rates, diffusion limits the movement of Na^+ ions due to time

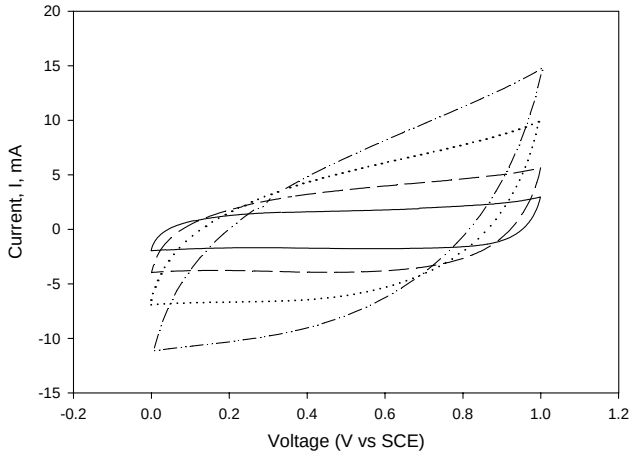

Fig. 5. CV curves of MnO_2 in 1 M NaCl electrolyte at 20 mV/s (- · · -), 10 mV/s (· · ·), 5 mV/s (- - -), 2 mV/s (—) scan rates.

constraint, and only the outer active surface is utilized for the charge storage. However, at lower scan rates, all the active surface area can be utilized for charge storage. Fig. 6a shows the plot of voltammetric charges as a function of the inverse of square root of the scan rate in 1 M NaCl electrolyte. By extrapolating scan rate to infinity, outer voltammetric charge (q_o^*) can be calculated. Fig. 6b shows the plot of voltammetric charges as the function of square root of the scan rate in 1 M NaCl electrolyte. By extrapolating to the zero scan rate, total voltammetric charge (q_T^*) can be determined. Outer voltammetric charge and total voltammetric charges are 21 and 155 C/g, respectively. The difference between outer and total voltammetric charges gives the inner voltammetic charge (q_i^*). Inner voltammetric charge corresponds to the inaccessible active surface area for the charge storage.

4.1.2. Electrochemical properties of as prepared material at different temperatures

Fig. 7 shows the CV curves for MnO_2 as prepared, dried at 250 and 400 °C for 5 h. The as prepared material and the material dried at 250 °C yielded the same specific

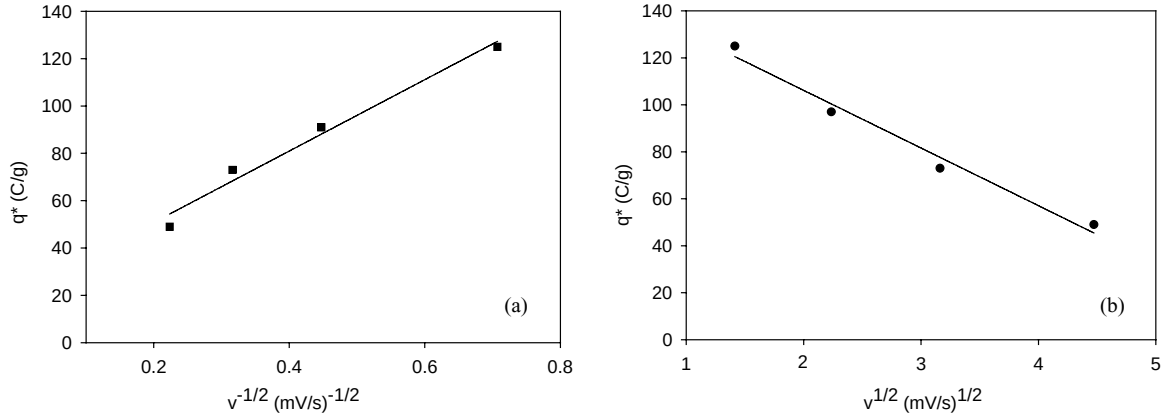

Fig. 6. Voltammetric charge vs. (a) inverse square root of scan rate and (b) square root of scan rate.

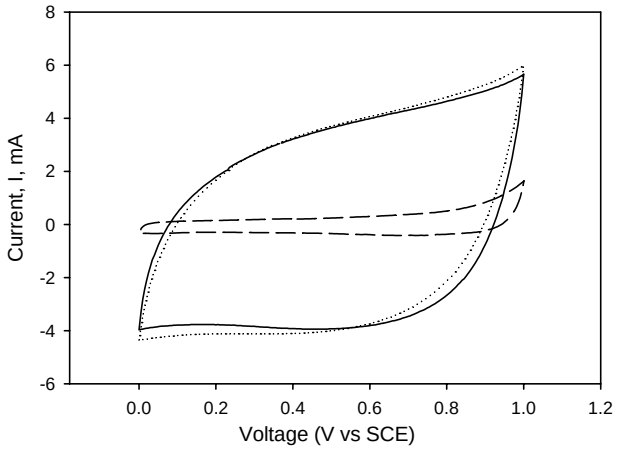

Fig. 7. CV curves of MnO_2 dried at different temperature, as prepared (—), 250 °C (· · ·), 400 °C (- - -) in 1 M NaCl electrolyte.

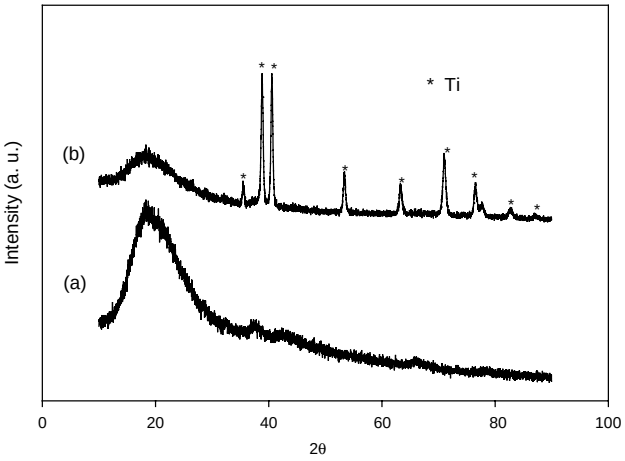

Fig. 9. XRD patterns of MnO_2 electrode (a) before cycling and (b) after cycling (Ti is the current collector).

capacitance, while MnO_2 dried at 400 °C showed a very low specific capacitance of 15 F/g. This variation cannot be explained based on surface area as the material remained amorphous till 400 °C. Chemically bound water is the only factor which may be playing a decisive role. Pseudocapacitance of oxide material depends on the water content [11,19]. Water content is essential for the transportation of active ionic species. In DTA studies, we observed the complete loss of water content at 270 °C. MnO_2 dried at 400 °C is left with no water content leading to the loss of pseudocapacitance.

4.1.3. Effect of cycling

Fig. 8a shows the effect of cycling on MnO_2 in 1 M NaCl solution at 5 mV/s scan rate up to 800 cycles. As indicated in the figure, cycling led to the rectangular shape. Specific capacitance as a function of cycling is shown in Fig. 8b. Specific capacitance remained constant up to 800 cycles. As we reported earlier, MnO_2 demonstrated capacitance fading after 200 cycles [2]. Fig. 9 shows XRD patterns of MnO_2 before and after cycling. Additional peaks were not detected in after cycling the material apart from the Ti peaks when compared to initial electrode material. The Ti peaks present material correspond to the Ti current collector. We believe the better performance of the present MnO_2 is due to its structural stability.

5. Conclusions

Amorphous MnO_2 was prepared by the sol–gel method in an ambigel form. The prepared material remained amorphous up to 400 °C. MnO_2 was transformed to crystalline Mn_2O_3 at 500 °C. This transformation was observed in both XRD and TGA/DTA analysis. The surface area of the as-prepared material was found to be 83 m^2/g. The composition of the material from TGA/DTA and ICP analysis was found to be $Na_{0.25}MnO_2{\cdot}0.5H_2O$. SEM images indicated agglomerated particles with an average size of about 5 μm.

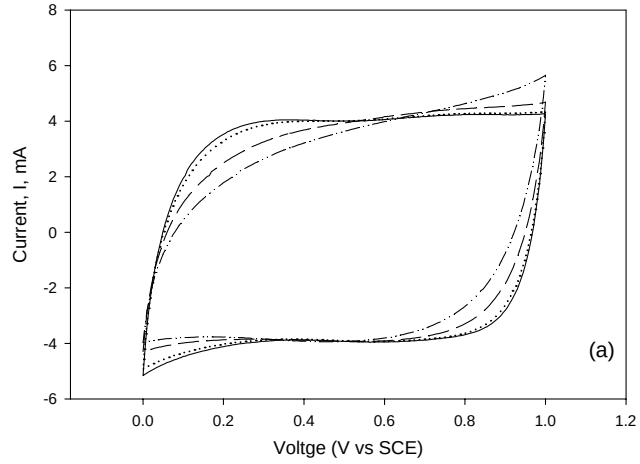

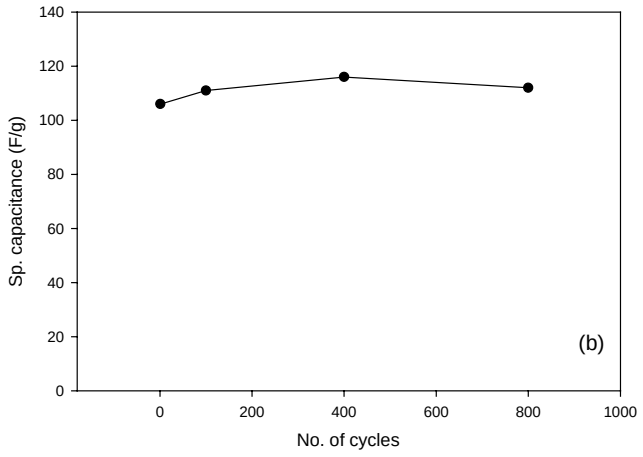

Fig. 8. (a) CV curves of MnO_2 in 1 M NaCl electrolyte at first cycle (- · · -), 100th cycle (- - -), 300th (· · ·), 400th (—). (b) Specific capacitance as a function of cycling.

MnO_2 showed ideal capacitative nature and yielded almost the same specific capacitance in 2 M NaCl and 2 M KCl electrolytes, whereas MnO_2 showed non-capacitative nature in 1 M Na_2SO_4 electrolyte. The maximum specific capacitance of 110 F/g was observed at a scan rate of 5 mV/s in 2 M NaCl solution. Comparable capacitance was obtained in 2 and 1 M NaCl solution. Outer and total voltammetric charge for MnO_2 were calculated to be 21 and 155 C/g, respectively, in 1 M NaCl. Cycling improved the performance of MnO_2 in 1 M NaCl electrolyte, and specific capacitance remained constant up to 800 cycles.

Acknowledgements

The authors are thankful for the financial support provided by National Science Foundation grant no. ECS-0099853. Special thanks to Dr. Divakar Mantha for the help rendered during the preparation of this manuscript.

References

[1] B.E. Conway, Electrochemical Supercapacitors, Kluwer Academic/Plenum Publishers, New York, NY, 1999.
[2] N. Reddy, G. Reddy, J. Power Sources 124 (2003) 330.
[3] R.N. Reddy, R.G. Reddy, Electrochemical capacitor and hybrid power sources, in: R.J. Brodd et al. (Eds.), The Electrochemical Society Proceedings Series, PV 2002–7, Pennington, NJ, 2002, p. 197.
[4] R.N. Reddy, R.G. Reddy, Fundamentals of advanced materials for energy conversion, in: D. Chandra, R.G. Bautista (Eds.), The Minerals, Metals & Materials Society, Warrendale, PA, 2002, p. 75.
[5] J.P. Zheng, T.R. Jow, J. Electrochem. Solid-state Lett. 2 (1999) 359.
[6] C. Lin, J.A. Ritter, B.N. Popov, J. Electrochem. Soc. 146 (1999) 3155.
[7] J.W. Long, A.L. Young, D.R. Rolison, J. Electrochem. Soc. 150 (2003) A1161.
[8] H.Y.Lee, V. Manivannan, J.B. Goodnough, C.R. Acad. Sci. Paris t. 2 serie II c (1999) 565.
[9] H.Y. Lee, J.B. Goodnough, J. Solid State Chem. 144 (1999) 220.
[10] Y.U. Jeong, A. Manthiram, J. Electrochem. Soc. 149 (2002) A1419.
[11] H. Kim, B.N. Popov, J. Electrochem. Soc. 150 (2003) D56.
[12] S.C. Pang, M.A. Anderson, T.W. Chapman, J. Electrochem. Soc. 147 (2000) 444.
[13] J.K. Chang, W.T. Tsai, J. Electrochem. Soc. 150 (2002) A1333.
[14] M. Toupin, T. Brousse, D. Belanger, Chem. Mater. 14 (2002) 3946.
[15] J. Yang, J.J. Xu, J. Power Sources 122 (2003) 180.
[16] R.N. Reddy, R.G. Reddy, Advanced materials for energy conversion II, in: D. Chandra, R.G. Bautista, L. Schlapbach (Eds.), The Minerals, Metals & Materials Society, Warrendale, PA, 2004, in press.
[17] S. Franger, S. Bach, J. Farcy, J.P. Pereira-Ramos, N. Baffier, J. Power Sources 109 (2002) 262.
[18] H.P. Stadniychuk, M.A. Anderson, T.W. Chapman, J. Electrochem. Soc. 143 (1996) 1629.
[19] J.P. Zheng, P.J. Cygan, T.R. Jow, J. Electrochem. Soc. 142 (1995) 2669.